






Comparative Study of Photocatalytic Performance of Nanocrystalline Bismuth Ferrite Synthesized Sol-gel and Hydrothermal Methods

Nurvet Kirkgecic^{1#} , Rabia Kirkgecic² , Handan Ozlu Torun³ , Serhan Urus² , and Mehmet S. Bozgeyik^{1,4#} 

Nanocrystalline Bismuth Ferrite (BiFeO₃, BFO) catalyst materials were synthesized using hydrothermal and sol-gel methods in order to examine the impact of crystallite size on photocatalysis. Crystal structures and optical properties were studied to explore photocatalytic performance. X-ray Diffraction analysis (XRD) showed that both synthesized samples were formed in pure BiFeO₃ without any secondary and impurity phases. The average crystallite size values calculated using the Debye-Scherrer formula were calculated as 39 nm and 46 nm for samples prepared by sol gel and hydrothermal methods, respectively. Photocatalytic activities of BFO nanocrystallite materials were studied by using methylene blue dyestuff water solution under a solar simulator. It was noted that the photocatalytic efficiency of BFO nanocrystallite synthesized by the sol gel method was higher compare to that of the synthesized by hydrothermal one. It was indicated that such an increase for the efficiency could be related with the dual effect of decreasing crystallite size and bandgap.

1. Introduction

Water is an indispensable vital natural resource for all organisms to survive. Factors such as the increase in world population and increasing urbanization and rapid industrialization based on technology have led to large-scale contamination of surface and groundwater resources in recent years [1, 2]. These contaminations contain many complex components, from organic pollutants to heavy metals and inorganic compounds. The main factors polluting water resources include synthetic dyes, which are frequently used in the textile, paper, pharmaceutical, leather and cosmetic industries [3]. These industrial synthetic dyes, which are released into the environment without adequate treatment, can be found in detectable amounts even at the lowest concentrations of water, and this can harm both human health and the aquatic ecosystem [4]. Considering that water resources are limited, important strategies such as effective and efficient use of water, prevention of water pollution, reuse

and recycling of water are emphasized. These strategies aim at supplying clean and healthy water to future generations, protecting ecosystems and meeting the needs of different water-related sectors. Traditionally, physical, chemical and biological techniques are widely used in the treatment of wastewater. The negative aspects of these techniques include secondary wastewater generation, lengthy procedures and high capital costs [5, 6]. Therefore, reliable, green, environmentally friendly, and cost-effective technologies should be developed and used urgently for environmental protection and sustainable growth [7]. In fact, photoactive materials sensitive to sunlight have the capacity to convert light into another form of energy such as mechanical, electrical and chemical energy [8]. For this reason, solar energy, which is a pioneer among renewable energy sources, has the potential to overcome many difficulties. In recent years, one of the most important applications that ensure the usability of solar energy is photocatalytic

¹Department of Physics, Faculty of Science, Kahramanmaraş Sutcu Imam University, 46050, Kahramanmaraş, Türkiye, ²Department of Chemistry, Faculty of Science, Kahramanmaraş Sutcu Imam University, 46050, Kahramanmaraş, Türkiye, ³Department of Energy System Engineering, Kahramanmaraş Istiklal University, 46300, Kahramanmaraş, Türkiye, ⁴Department of Materials Science and Engineering, Graduate School of Natural and Applied Science, Kahramanmaraş Sutcu Imam University, 46050, Kahramanmaraş, Türkiye

#Corresponding authors: nurvetkrgct@gmail.com, msbozgeyik@yahoo.com

Keywords: Photocatalyst; Bismuth Ferrite; Nanocrystalline Materials; Nanosized Crystallite; Bandgap.

Received: 03 October 2023 | Accepted: 27 February 2024 | Published online: 30 June 2024

J.NanoSci.Adv.Mater. 2024, 3 (1), 1

degradation. Photocatalytic degradation is a process in which a chemical reaction takes place under the influence of light energy and a semiconductor photocatalyst. Photocatalysis, which is an advanced oxidation process, stands out as a technique that is rapidly spreading and gaining more importance every day [9]. Unlike traditional methods, the photocatalytic technique offers an environmentally friendly, fast, and economical solution in wastewater treatment. This technique can provide full mineralization of non-biodegradable organic pollutants, can be operated at ambient temperature and pressure, and has the advantages of low operating cost, without generating secondary pollution [10]. Many scientific studies have been carried out for the selection of photocatalysts sensitive to visible light with high efficiency. Among the photocatalyst materials commonly used in this field are TiO₂ (3.3 eV), ZnS (3.6 eV), ZnO (3.4 eV), SrTiO₃ (2.97 eV) and α-Fe₂O₃ (2.67 eV) semiconductor [11]. The more environmental and energy problems increase, the more material properties need to be improved. Regarding practical and device applications, semiconductors are the most popular materials which researchers adhere [12]. However, these broad-bandgap semiconductor oxides can only absorb 5% of the sunlight in the ultraviolet (UV) region, an important factor that critically limits their applicability. Recently, Bismuth ferrite (BiFeO₃, BFO), an ABO₃ perovskite type oxide with a bandgap of 2.2–2.7 eV, is one of the compounds investigated as a potential optical material for photocatalytic applications [13]. Bismuth ferrite, which has multifunctional properties, has a wide range of applications. Due to its superior electrical, magnetic and optical properties, it is an important engineering material that is promising in meeting the demands of the high-tech industry, such as the design of next-generation electronic, magnetic and optoelectronic devices [14, 15]. While BiFeO₃ is indeed a significant candidate for visible light photocatalysis, its photocatalytic efficiency is primarily hindered by the high recombination rate of electron-hole pairs and the relatively low conduction band level [16]. The efficiency and photocatalytic activity of BFO photocatalyst are directly affected by many factors such as electronic band structure, surface morphology, particle size, porosity and surface area that affect the separation of e⁻/h⁺ pairs and optical absorption properties [17, 18].

This study was conducted to evaluate the effect of changing crystallite sizes of BFO synthesized using sol-gel and hydrothermal methods on the photocatalytic activity.

2. Results and Discussion

X-ray Diffraction analysis (XRD) technique is an important structural analysis method used to confirm the phase formations that occur after the synthesis of nanocrystalline materials. XRD technique was used to examine the structural phase analysis of BFO nanocrystalline materials obtained by different synthesis methods. Average crystallite size calculations, phase and peak analysis of the samples were determined X'Pert High Score Plus program. The mean crystal size of the samples was determined based on XRD peak pattern data by using Debye–Scherrer formula:

$$D_c = \kappa\lambda / \beta \cos\theta \quad (1)$$

Here, D_c represents the average crystal size, λ denotes the X-ray wavelength, and β (FWHM) stands for the width of the diffraction peak at half-maximum for the diffraction angle (2θ).

Figure 1 shows the XRD diffraction pattern of BFO samples synthesized by sol gel and hydrothermal methods. It was clearly seen that both samples were well crystallized in polycrystalline form.

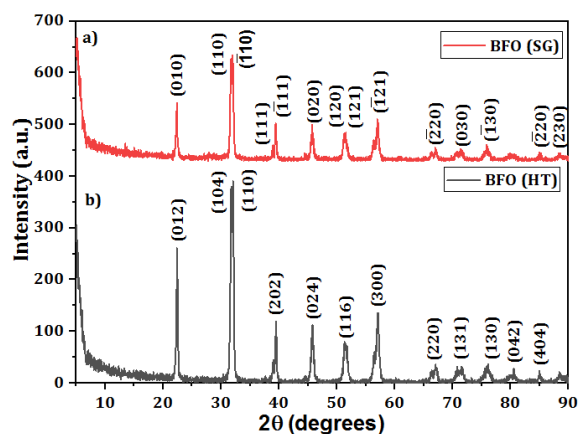


Figure 1. XRD patterns of BFO nanocrystalline materials prepared by a) sol gel b) hydrothermal methods.

The sample synthesized by the sol gel method is BiFeO₃ in the main phase and its crystal structure is rhombohedral with R-3m space group without any impurity and secondary phases (Figure 1 a). All peaks of XRD are compatible with ICSD card no: 01-072-2112. The average crystallite size was calculated from the Debye–Scherrer equation using all diffraction peaks at approximately 39 nm.

The XRD peaks of the BFO prepared by the hydrothermal method are compatible with the standard main phase BiFeO₃ which has a

rhombohedral structure with the R3c space group [ICSD card no. 01-086-1518] (Fig. 1b). There was no secondary and impurity phase formed. The mean crystallite size was calculated as 46 nm.

Nanocrystalline high pure BFO was successfully synthesized by both sol-gel and hydrothermal methods. Sharp diffraction peaks clearly reflect crystalline particle formation. The expansion and relative density of the patterns vary depending on changing experimental conditions. This refers to changes in the grain size of the prepared nanostructures [19]. An increase in the XRD diffraction peak intensity and a decrease in FWHM of the BFO sample prepared by the hydrothermal method were observed, indicating an increase in crystal size according to the Scherrer equation [20]. This explains the increased grain growth and better crystallization of the sample [21].

Considering a candidate semiconductor material for practical and device applications electronic and optical properties are critically important for electron-hole pair formation, exciton lifetime and recombination physical measurable [22]. UV-vis spectrometry technique was used to evaluate the visible light response and bandgap BFO nanocatalysts. Studying optical absorption is very important since the UV-vis absorption edge depends on the energy band of a semiconductor catalyst [23].

Forbidden bandgap of a semiconductor is determined by using Tauc equation,

$$(\alpha h\nu)^n = A(E_g - h\nu) \quad (2)$$

[24]. Here, α is the absorption coefficient, and $h\nu$ is the energy of the incident photon, E_g refers to the bandgap, A is a scaling constant, while n is a factor dependent on the type of semiconductor material. Bismuth ferrite is a direct bandgap semiconductor, so n is taken as 2. Figure 2 shows the bandgap calculation using Tauc plot of the BFO sample prepared by the hydrothermal method.

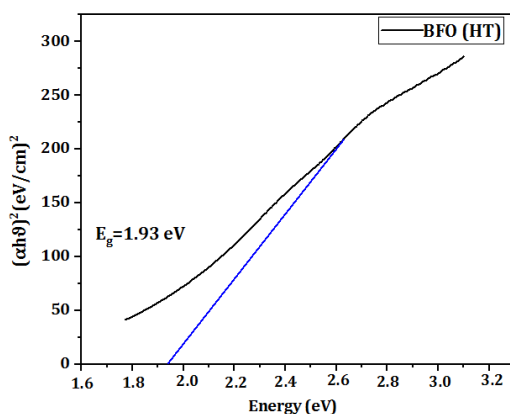


Figure 2. Tauc plot of nanocrystalline BFO prepared by hydrothermal method.

Absorption edges determine the wavelength at which a material can absorb photons and initiate electronic transitions. BFO nanocrystalline catalysts prepared by hydrothermal method has a strong photoabsorption in the wavelength range of 400-700 nm. This indicates a remarkable response in the visible light region. The absorption edge of BFO nanocrystalline material prepared by hydrothermal method is approximately 665 nm. Using Tauc's plotting method, the bandgap value was calculated as $E_g = 1.93$ eV. The band gap value is quite close to other reports: 1.96 eV, 1.94 eV, 1.8 eV, 1.93 eV [25, 26, 27, 28].

Figure 3 shows the bandgap calculation of BFO sample prepared by sol-gel technique.

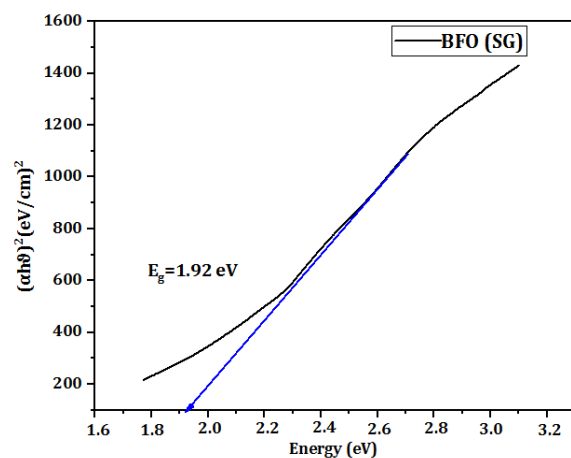


Figure 3. Tauc graph of BFO sample BFO nanocrystalline material synthesized by sol-gel method.

The bandgap absorption edge of the BFO nanocrystallite catalyst prepared by the sol-gel method is around 671 nm. The forbidden band gap value was determined as $E_g = 1.92$ eV. According to previous reports, the narrowing of the band gap in BFO nanopowders prepared by the sol-gel method can be directly attributed to the decrease in crystallite size [29]. As the crystallite size decreases, a simultaneous decrease in the band gap is observed.

In order to determine the photocatalytic activity of the synthesized catalysts, the degradation efficiency of an aqueous solution containing methylene blue without BFO nanocrystallite was first tested. Then, BFO nanocrystallite materials were used as catalysts in methylene blue aqueous solution. These measurements were carried out under a solar simulator in the wavelength range of 400-800 nm, within a 10 minutes time period starting from 0 minutes to 120 minutes.

Figure 4 shows the absorbance and wavelength change graph of methylene blue aqueous solution in daylight in a closed environment without sunlight.

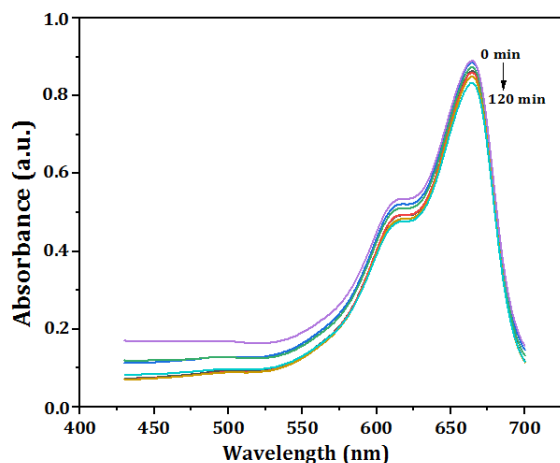


Figure 4. Absorbance of an aqueous solution of methylene blue (daylight) without catalyst.

In the aqueous solution of methylene blue without catalyst, no obvious change was observed for the measurements starting from 0 min to 120 min, as seen in Figure 5. The efficiency of 4 % was obtained in sole methylene blue aqueous solution.

Figure 5 shows the absorbance and wavelength variation graph of sole methylene blue aqueous solution without catalyst recorded under the solar simulator.

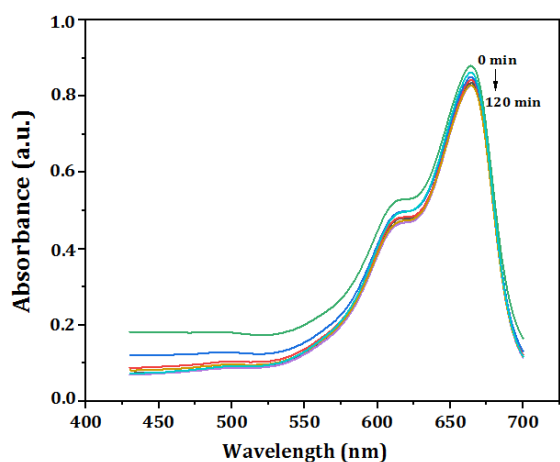


Figure 5. Absorbance of the aqueous solution of methylene blue (sunlight) without catalyst.

The absorbance of the methylene blue aqueous solution without catalyst did not show any significant change under the solar simulator. The photocatalytic degradation efficiency was calculated as 6 %.

Figure 6 shows the wavelength dependent absorbance graph of the hydrothermally synthesized BFO photocatalyst added aqueous solution of methylene blue.

The degradation of the BFO photocatalyst prepared by the hydrothermal method on the methylene blue dyestuff was calculated as 45 %

from equation (3).

$$\text{Degradation \%} = \frac{C_0 - C_t}{C_0} \times 100 \quad (3)$$

where C_0 and C_t (mg/l) are the initial and concentration at time t (mg/l). This process was repeated for each sample.

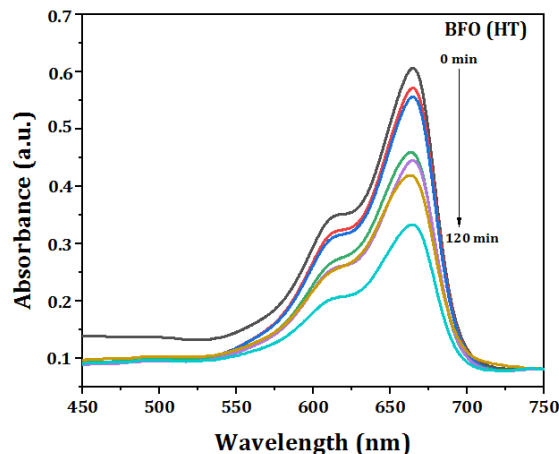


Figure 6. Absorbance of hydrothermally synthesized BFO nanocrystallite photocatalyst added aqueous solution of methylene blue.

The photocatalytic reaction basically involves three main processes: First, the formation of excitons (electron-hole pairs) as a result of the absorption of light by photocatalysts; then separating and transporting these charges to the photocatalyst surface; and finally, the reduction and oxidation reactions that take place on the photocatalyst surface [30]. The high efficiency of the photocatalyst is based on a combination of four key elements such as light absorption capacity, density of active sites, redox capacity and light-triggered electron-hole recombination rate. The fast recombination rate of photogenerated electron-hole pairs causes the photocatalytic efficiency to decrease [31].

Figure 7 shows the wavelength dependent absorbance of the sol-gel synthesized BFO photocatalyst.

The degradation percent of the BFO photocatalyst prepared by the sol gel method on the methylene blue dyestuff was calculated from equation 3 as 50 %. Figure 7 clearly shows the decrease in absorbance with increasing irradiation time, showing the degradation of methylene blue. BFO nanoparticles produced by the sol-gel method exhibit a higher photocatalytic activity compared to powders obtained by the hydrothermal method. The efficiency of photocatalysts depends on factors such as crystallite size, morphology, surface area and bandgap [32]. The improvement of photocatalytic performance in BFO nanocrystallite

Table 1. Crystallite size, bandgap values and photocatalytic degradation of synthesized photocatalysts

BFO Nanocrystallite Photocatalyst Synthesized by	Sol-gel	Hydrothermal
Crystallite size (nm)	39	46
Bandgap value (eV)	1.92	1.93
Degradation (%)	50	45

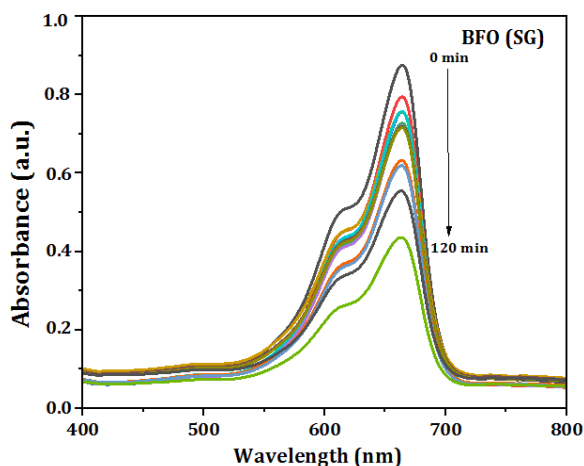


Figure 7. Absorbance of the sol-gel synthesized BFO nanocrystallite photocatalyst in methylene blue.

may be due to the decreasing bandgap value and crystallite size [33]. Since the size of the nanoparticles acts as photocatalysts, the large surface area resulting from the small crystals may have enhanced the reactions occurring on the surface leading to increased photocatalytic activity [34].

Table 1 shows the crystallite size, photocatalytic degradation, and bandgap values of the synthesized BFO photocatalysts.

3. Conclusion

BFO nanocrystallite materials were synthesized by sol-gel and hydrothermal methods. Successful synthesized pure BFO polycrystalline without any secondary phase was confirmed by the XRD analysis. It was observed that the photocatalysts synthesized different methods with different structural properties exhibit different in visible light absorption properties and forbidden bandgap values. Photocatalytic degradations of BFO catalysts synthesized by hydrothermal and sol gel methods were determined as 45 % and 50 %, respectively. The increased photocatalytic performance of BFO nanocrystallite prepared by the sol gel method was associated with reduced crystallite size and narrow bandgap. It can be concluded that the both

crystallite size and bandgap have critical effect on the photocatalytic performance. These findings allow us to conclude that the BFO nanocrystallite has a significant potential for photocatalytic applications upon variation of crystallite size and bandgap.

Method

Preparation of BFO photocatalysts by sol gel method: Bismuth nitrate $[\text{Bi}(\text{NO}_3)_3 \cdot 5\text{H}_2\text{O}]$, Iron nitrate $[\text{Fe}(\text{NO}_3)_3 \cdot 9\text{H}_2\text{O}]$, Nitric acid (HNO_3) and Tartaric acid ($\text{C}_4\text{H}_6\text{O}_6$) were used as starting chemicals to synthesize pure Bismuth ferrite. Firstly, bismuth nitrate and iron nitrate powders were weighed according to 0.001 mol ratio. Weighed powders were added to 10 mL of distilled water. Then, some nitric acid was added dropwise with a magnetic stirrer. After dissolution was completed, an appropriate amount of tartaric acid was added to the solution as the chelating agent. The resulting solution was stirred on a magnetic stirrer until it turned into a sol-gel at a certain temperature. The resulting gel was heat treated in an ash oven for 1 hour at 140°C for drying. Afterwards, the obtained product was placed in the crucible and calcined at 500°C for 1 hour.

Preparation of BFO photocatalysts by hydrothermal method: Bismuth nitrate $[\text{Bi}(\text{NO}_3)_3 \cdot 5\text{H}_2\text{O}]$, Iron nitrate $[\text{Fe}(\text{NO}_3)_3 \cdot 9\text{H}_2\text{O}]$, Nitric acid (HNO_3), Potassium nitrate (KNO_3) and Potassium hydroxide (KOH) were used as starting chemicals. The powders weighed 0.005 mol $\text{Bi}(\text{NO}_3)_3$ and 0.005 mol $\text{Fe}(\text{NO}_3)_3$ were dissolved in diluted HNO_3 (nitric acid) to form a solution. A clear solution was observed without any visible suspension and sediment. 50 ml of KOH solution with a molar concentration of 12M was added dropwise with magnetic stirring until brown precipitate formed. The solution was filtered and washed with distilled water to remove NO_3^- and K^+ ions. It was dried in an oven at 70°C for 4 hours. The precipitate was then mixed with 40 ml of KOH solution (12M), followed by the addition of 10 g of KNO_3 under constant stirring for 5 minutes. The solution was transferred to a 90 mL Teflon beaker and placed in a stainless steel autoclave with an inner liner. The mixture was kept in the hydrothermal device at 200°C for 24 hours. After cooling to room temperature, the product at the bottom was washed with distilled water until the pH value was 7 and then dried at 70°C .

Structural Analysis: The synthesized BFO catalysts were characterized by Philips X'Pert Promodel device ($\lambda=0.154056$ nm, Cu-Ka radiation) using X-Ray diffraction (XRD) technique to calculate average crystallite sizes, phases and peak analysis. XRD measurements

were performed over a scanning angle range of $5^\circ \leq \theta \leq 95^\circ$.

Photocatalytic Activity Measurements: To examine the photocatalytic performance of the synthesized BFO nanocrystalline material, methylene blue was used as a model pollutant dyestuff. First, a 5 mg methylene blue powder sample was weighed using a precision digital balance and then transferred to a capped glass tube. First, a solution of 5 ppm methylene blue (MB) was mixed in 200 ml of distilled water until it was completely dissolved. Then, 10 mg of photocatalyst powder sample and 5 ppm methylene blue solution were homogeneously suspended in 50 mL of aqueous solution. In order to ensure equilibrium adsorption on the surface of the catalyst, the aqueous solution was kept in the dark for 30 minutes before illumination. For measurements, 2 ml samples were taken from the solutions. Before measurement, the particulate samples were spun in the centrifuge. Shimadzu UV spectrophotometer (Model: UV-1800) was used to examine the absorbance properties of solution samples. Measurements were made in the wavelength range of 400 - 800 nm and were repeated every 10 minutes, taking 0 minutes as the starting point. After 120 minutes of measurement, the process was terminated. Methylene blue visible wavelength = 664 nm. The percent photocatalytic degradation of the samples was determined according to equation (3).

Bandgap measurement: Initially, 10 mg of powder sample was precisely weighed using a precision digital balance and taken into the glass tube. After adding stoichiometric amounts of ethyl alcohol to the sample, the ethyl alcohol aqueous solution was stirred in an ultrasonic water bath for approximately 2 min. After the process was completed, measurements were taken using a UV-vis spectrophotometer. Absorption spectrum scan was taken between 200-900 nm.

Acknowledgements

The corresponding authors acknowledge Kahramanmaraş Sutcu Imam University for the financial support of the postdoctoral research project of DOSAP-2022/5-18.

Authors' contributions:

Corresponding authors contributed to conducting research by means of synthesis, characterizations, and interpretations of the data as well as design the article. Other authors contributed to the limited laboratory facilities and helped in photocatalysis.

Data Availability Statement

The data of the current article is not available without permission.

References

- [1] Gómez-Pastora, J., Dominguez, S., Bringas, E., Rivero, M. J., Ortiz, I., & Dionysiou, D. D., Review and perspectives on the use of magnetic nanophotocatalysts (MNPCs) in water treatment. *Chemical Engineering Journal*, **310**, 407-427 (2017).
- [2] Jamaludin, N., Razak, N. A. A., Ismail, F. D., & Chaudhary, K. T., Photocatalytic degradation of rhodamine B dye under visible light using cerium-cobalt co-doped bismuth ferrite nanoparticles. In *Journal of Physics: Conference Series*, **2432**(1), 012015 (2023).
- [3] Orudzhev, F., Sobola, D., Ramazanov, S., Částková, K., Papež, N., Selimov, D. A. & Holcman, V., Piezo-enhanced photocatalytic activity of the electrospun fibrous magnetic PVDF/BiFeO₃ membrane. *Polymers*, **15**(1), 246 (2023).
- [4] Nazeer, Z., Bibi, I., Majid, F., Kamal, S., Arshad, M. I., Ghafoor, A., & Iqbal, M., Optical, Photocatalytic, Electrochemical, Magnetic, Dielectric, and Ferroelectric Properties of Cd-and Er-Doped BiFeO₃ Prepared via a Facile Microemulsion Route. *ACS omega*, **8**(28), 24980-24998 (2023).
- [5] Sharmin, F., & Basith, M. A., Highly efficient photocatalytic degradation of hazardous industrial and pharmaceutical pollutants using gadolinium doped BiFeO₃ nanoparticles. *Journal of Alloys and Compounds*, **901**, 163604 (2022).
- [6] Ren, G., Han, H., Wang, Y., Liu, S., Zhao, J., Meng, X., & Li, Z., Recent advances of photocatalytic application in water treatment: A review. *Nanomaterials*, **11**(7), 1804 (2021).
- [7] Tong, H., Ouyang, S., Bi, Y., Umezawa, N., Oshikiri, M., & Ye, J., Nano-photocatalytic materials: possibilities and challenges. *Advanced materials*, **24**(2), 229-251 (2012).
- [8] Butler, K. T., Frost, J. M., & Walsh, A., Ferroelectric materials for solar energy conversion: photoferroics revisited. *Energy & Environmental Science*, **8**(3), 838-848 (2015).
- [9] Gaur, A., Sharma, M., Chauhan, V. S., & Vaish, R., Visible light photocatalytic activity in BiFeO₃ glass-ceramics. *Materials Chemistry and Physics*, **303**, 127710 (2023).
- [10] Lam, S. M., Sin, J. C., & Mohamed, A. R., A newly emerging visible light-responsive BiFeO₃ perovskite for photocatalytic applications: a mini review. *Materials Research Bulletin*, **90**, 15-30 (2017).
- [11] Zhang, F., Wang, X., Liu, H., Liu, C., Wan, Y., Long, Y., & Cai, Z., Recent advances and applications of semiconductor photocatalytic technology. *Applied Sciences*, **9**(12), 2489 (2019).
- [12] Karataş, Ş., Effect of perylenetetracarboxylic dianhydride on the main electrical properties and interface states of Al/p-Si structures. *Physica B: Condensed Matter*, **657**, 414790, (2023).
- [13] Zhou, T., Zhai, T., Shen, H., Wang, J., Min, R., Ma, K., & Zhang, G., Strategies for enhancing performance of perovskite bismuth ferrite photocatalysts (BiFeO₃): A comprehensive review. *Chemosphere*, **339**, 139678 (2023).
- [14] Basith, M. A.; Kurni, O.; Alam, M. S.; Sinha, B. L.; Ahmmad, B. Room temperature dielectric and magnetic properties of Gd and

Ti co-doped BiFeO₃ ceramics, *Journal of Applied Physics*, **115**, 024102 (2014).

[15] Sun, M.; Bai, L.; Ma, W.; Liu, Y.; Zhang, J.; Yang, J. Ho and Ti Co-Substitution Tailored Structural Phase Transition and Enhanced Magnetic Properties of BiFeO₃ Thin Films. *ACS Omega*, **5**, 29292–29299 (2020).

[16] Irfan, S., Zhuanghao, Z., Li, F., Chen, Y. X., Liang, G. X., Luo, J. T., & Ping, F., Critical review: Bismuth ferrite as an emerging visible light active nanostructured photocatalyst. *Journal of Materials Research and Technology*, **8**(6), 6375–6389 (2019).

[17] Supriya, S., Recent trends and morphology mechanisms of rare-earth based BiFeO₃ nano perovskites with excellent photocatalytic performances, *Journal of Rare Earths*, **41**(3), 331–341 (2022).

[18] Gao, T., Chen, Z., Huang, Q., Niu, F., Huang, X., Qin, L., & Huang, Y., A review: preparation of bismuth ferrite nanoparticles and its applications in visible-light induced photocatalyses. *Reviews on Advanced Materials Science*, **40**(2), 97–109 (2015).

[19] Remya, K. P., Prabhu, D., Joseyphus, R. J., Bose, A. C., Viswanathan, C., & Ponpandian, N., Tailoring the morphology and size of perovskite BiFeO₃ nanostructures for enhanced magnetic and electrical properties. *Materials & Design*, **192**, 108694 (2020).

[20] Hassanzadeh-Tabrizi, S. A., Precise calculation of crystallite size of nanomaterials: a review. *Journal of Alloys and Compounds*, **968**, 171914 (2023).

[21] Dhanya, S. R., Nair, S. G., Satapathy, J., & Kumar, N. P., Structural and spectroscopic characterization of bismuth-ferrites. *AIP Conference Proceedings*, **2166** (1), (2019).

[22] Seymen, H., Berk, N., Orak, I., & Karataş, Ş., Effect of illumination intensity on the electrical characteristics of Au/SiO₂/n-type Si structures with GO and P3C4MT interface layer. *Journal of Materials Science: Materials in Electronics*, **33**(24), 19656–19666, (2022).

[23] Gao, F., Chen, X. Y., Yin, K. B., Dong, S., Ren, Z. F., Yuan, F., & Liu, J. M., Visible-light photocatalytic properties of weak magnetic BiFeO₃ nanoparticles. *Advanced materials*, **19**(19), 2889–2892 (2007).

[24] Tauc, J., Grigorovici, R., & Vancu, A, Optical properties and electronic structure of amorphous germanium. *Physica Status Solidi (B)*, **15**(2), 627–637 (1966).

[25] Rouhani, Z., Karimi-Sabet, J., Mehdipourghazi, M., Hadi, A., & Dastbaz, A., Response surface optimization of hydrothermal synthesis of Bismuth ferrite nanoparticles under supercritical water conditions: Application for photocatalytic degradation of Tetracycline. *Environmental Nanotechnology, Monitoring & Management*, **11**, 100198 (2019).

[26] Chen, X. Z., Qiu, Z. C., Zhou, J. P., Zhu, G., Bian, X. B., & Liu, P., Large-scale growth and shape evolution of bismuth ferrite particles with a hydrothermal method. *Materials Chemistry and Physics*, **126**(3), 560–567 (2011).

[27] Tong, T., Cao, W., Zhang, H., Chen, J., Jin, D., & Cheng, J., Controllable phase evolution of bismuth ferrite oxides by an organic additive modified hydrothermal method. *Ceramics International*, **41**, S106–S110 (2015).

[28] Djatoubai, E., Khan, M. S., ul Haq, S., Guo, P., & Shen, S., Rational design of BiFeO₃ nanostructures for efficient charge carrier transfer and consumption for photocatalytic water oxidation. *Journal of Alloys and Compounds*, **911**, 164920 (2022).

[29] Matin, M. A., Rhaman, M. M., Hossain, M. N., Mozahid, F. A., Hakim, M. A., Rizvi, M. H., & Islam, M. F., Effect of preparation routes on the crystal purity and properties of BiFeO₃ nanoparticles. *Transactions on Electrical and Electronic Materials*, **20**(6), 485–493 (2019).

[30] Srivastav, S. K., Singh, S. P., & Kumar, K., Perovskite BiFeO₃ Nanostructure Photocatalysts for Degradation of Organic Pollutants. *Nanomaterials and Nanocomposites for Environmental Remediation*, 141–162 (2021).

[31] Nazeer, Z., Bibi, I., Majid, F., Kamal, S., Ghafoor, A., Ali, A., ... & Iqbal, M., Microemulsion synthesis of Ga and Sr doped BiFeO₃ nanoparticles and evaluation of their ferroelectric, optical, dielectric and photocatalytic properties. *Physica B: Condensed Matter*, **657**, 414788 (2023).

[32] Maleki, H., Photocatalytic activity and magnetic enhancements by addition of lanthanum into the BiFeO₃ structure and the effect of synthesis method. *Journal of Materials Science: Materials in Electronics*, **29**(14), 11862–11869 (2018).

[33] Kebede, M. T., Devi, S., Dillu, V., & Chauhan, S., Rhombohedral distortion induced structural, magnetic, optical phase transitions and photocatalytic activity in Sm and Sm-Cr co-substituted bismuth ferrite nanoparticles. *Journal of Crystal Growth*, **620**, 127336 (2023).

[34] Reddy, B. P., Rajendar, V., Shekar, M. C., & Park, S. H., Particle Size Effects on the Photocatalytic Activity of BiFeO₃ Particles. *Digest Journal of Nanomaterials & Biostructures (DJNB)*, **13**(1), 87–95 (2018).